Model-Based Compensation of Topographic Effects for Improved Stem-Volume Retrieval From CARABAS-II VHF-Band SAR Images

Klas Folkesson, Gary Smith-Jonforsen, and Lars M. H. Ulander, *Senior Member, IEEE*

***Abstract*—A limiting factor that has been identified for stem-volume retrieval in coniferous forests using VHF synthetic aperture radar is that the backscatter varies depending on ground topography. On sloping ground, the backscatter from a forest is reduced, since the dominant ground–trunk double-bounce scattering mechanism is changed. This leads to underestimation of stem volume, and the variations caused by topography can obscure real variations in stem volume. By using multiple images acquired with different flight headings and combining the image information with ground-topography data in a model-based inversion method, we are able to compensate for the ground-topography influence on the backscatter. The inversion method is based on image segmentation and the optimal estimation method. Using four or more images from the CARABAS-II system and a coarse digital elevation model with 50-m horizontal grid, the stem volume can be retrieved with an average root-mean-square error (rmse) of less than 60 $\mathrm{m^3ha^{-1}}$ for stem volumes in range of 80–700 $\mathrm{m^3ha^{-1}}$ (in terms of above-ground biomass, this is equivalent to an rmse of less than 40 ton $\cdot$ $\mathrm{ha^{-1}}$ over the range of 50–400 ton $\cdot$ $\mathrm{ha^{-1}}$). The retrieval accuracy is similar to that previously obtained for similar forests standing on flat and horizontal ground.**

***Index Terms*—Forestry, image segmentation, synthetic aperture radar (SAR), VHF measurements, VHF radar.**

I. Introduction

FOREST BIOMASS retrieval is one of the most promising applications of long-wavelength synthetic aperture radar (SAR). In particular, VHF SAR has shown promising results [1]–[9], where the problem of signal saturation for high biomass levels that affects optical remote sensing and high-frequency SAR is avoided. The lack of saturation is due to the ability of VHF waves to penetrate the foliage and that the backscatter comes primarily from tree trunks, where most of the biomass is stored. An alternative to measuring biomass is to use stem volume, which is also a more common measure of forest inventory for forest companies in Scandinavia. The stem volume is the volume of stems including bark but excluding branches, needles, and stumps and is measured in cubic meters per hectare. For Scandinavian conditions, the stem volume is related to the dry biomass as 100 $\mathrm{m^3ha^{-1}} \approx 60$ ton $\cdot$ $\mathrm{ha^{-1}}$ [10].

CARABAS-II is an airborne SAR system developed by the Swedish Defence Research Agency (FOI) [11] and operating in the lower VHF-band (20–90 MHz). Shortly after the first flights with the first generation of CARABAS-I in 1992, it was observed that the backscatter was closely related to forest stem volume [1]. These first results were obtained for broadleaf oak forest, while later, measurements have been focused toward coniferous forest. For coniferous forests, the accuracy of stem-volume retrieval has been reported to be as high as 49 $\mathrm{m^3ha^{-1}}$ for stem volumes ranging from 100 to 600 $\mathrm{m^3ha^{-1}}$ [12]. Below 100 $\mathrm{m^3ha^{-1}}$, the sensitivity is low due to weak backscatter, and hence a low signal-to-noise ratio, but for higher stem volumes, the stem volume is highly correlated with the CARABAS-II backscatter [4]. No saturation for stem volumes up to 900 $\mathrm{m^3ha^{-1}}$ has been observed [6].

An important feature of CARABAS-II for stem-volume retrieval is not only the good foliage penetration but that the backscattering strength is directly related to the stem volume. On flat and horizontal ground, the backscattering from a vertical stem consists mainly of four components, i.e., direct stem, ground–stem, stem–ground, and ground–stem–ground [5], [13]. Depending on incidence angle, dielectric constant, and stem height, one or more of these mechanisms may dominate. In this paper, we consider incidence angles in the range of $46^\circ - 66^\circ$ for which the two double-bounce components (ground–stem and stem–ground) dominate for stem heights larger than about 5 m [5]. The Rayleigh–Gans approximation may be used to show that the radar cross section of a dielectric stem over a dielectric ground plane is proportional to the squared volume of the stem, provided that the radius a and length l fulfils $ka \ll 1$ and $l/a > 20\sqrt{\epsilon_r}$, where k is the wavenumber and ϵ_r ($\sim$10–15) is the relative dielectric permittivity of the trunks. The backscattering coefficient is therefore proportional to the sum of the squared volumes per unit area, assuming that the stems are randomly positioned. An even simpler model may be obtained if the individual stems can be resolved in the images; in which case, the backscatter amplitude s^o is proportional to the sum of the volumes per unit area, i.e., the (average) stem volume [5]. Individual stems in dense forest are usually unresolved in standard CARABAS-II images, although in some special cases, it is possible to improve the resolution to better than 1 m, in which case, most stems

Manuscript received December 19, 2007; revised April 30, 2008. Current version published March 27, 2009. This work was supported by the Swedish National Space Board.

K. Folkesson is with the Department of Radio and Space Science, Chalmers University of Technology, 412 96 Göteborg, Sweden (e-mail: klas.folkesson@chalmers.se).

G. Smith-Jonforsen was with the Department of Radio and Space Science, Chalmers University of Technology, 412 96 Göteborg, Sweden. He is now with Saab AB, Saab Microwave Systems, 412 89 Göteborg, Sweden.

L. M. H. Ulander is with the Department of Radio and Space Science, Chalmers University of Technology, 412 96 Göteborg, Sweden, and also with the Department of Radar Systems, Swedish Defence Research Agency, 581 11 Linköping, Sweden.

Digital Object Identifier 10.1109/TGRS.2008.2009531

in mature forests are resolved [8]. Nevertheless, backscatter amplitude has experimentally been observed to be proportional to stem volume even if the individual stems are not resolved [14]. This is probably caused by the high correlation observed between mean-squared volume and mean volume squared in the forests that have been studied.

A problem that has been identified for stem-volume retrieval using VHF SAR is that the backscatter varies depending on ground topography [7]. This is because the ground–trunk double-bounce scattering dominates. On sloping ground, the backscatter from a forest is reduced, since trees usually have trunks close to vertical and sloping ground changes the dihedral scattering mechanism [15]. The change in backscatter depends also on the direction of the slope relative to the radar look direction. Therefore, the effects of slopes can lead to underestimation of stem volume, and the variations caused by topography can also obscure variations in stem volume.

Retrieving stem volume from VHF images using simple inversion methods, e.g., directly relating average backscatter to stem volume, will lead to underestimation in areas with sloping ground. This can be mitigated if multiple images from different flight directions are available. In [7], a heuristic method was proposed for stem-volume retrieval in sloping terrain. The method proposed was to find which of the multiple images gave the highest backscatter, and then, assuming that this was reasonably close to the backscatter that would be obtained from the same stem volume on horizontal ground. To reduce the effects of statistical fluctuations in the images, the stands were first divided into segments using a digital elevation model (DEM) to find areas with constant slope. For each segment, the average backscatter was calculated for each image, and the highest backscatter value was selected and converted to stem volume for that segment using an empirical regression function. The results showed that this method could significantly improve the stem-volume estimation accuracy over that obtained from a single image.

To further our understanding of the effects of sloping terrain on CARABAS-II images, modeling work has been performed. In [15], an electromagnetic scattering model was used to investigate scattering, and a semiempirical model proposed to describe the variations in backscatter from vertical stems caused by topography. This model was further analyzed in [14], where measurements were used to show that the semiempirical forward model could often be used to explain measurements of CARABAS-II backscatter to an accuracy similar to that obtained on flat, horizontal ground. However, to realize the full potential of CARABAS-II for stem-volume mapping requires the development of inversion algorithms. This is the purpose of this paper.

To improve stem-volume estimation on sloping ground, this paper investigates new methods for combining CARABAS-II data from multiple flight directions. First, the images are divided into segments using an automatic algorithm based solely on the image data. This is believed to be an improvement on the approach used in [7], as it is independent of a DEM and also includes variations in forest properties, so that segments more closely follow the natural variations in both forest properties and ground topography. Second, we propose a method using model-based inversion, where data from all available images are combined to estimate stem volume using the optimal estimation method [16]. This has the potential advantage over simply using the highest backscatter of being more robust to errors caused by strong backscatter, e.g., from man-made objects in the forest or imaging artifacts. In addition, the model-based method is expected to be less sensitive to the exact choice of flight directions, and an intrinsic estimate of the retrieval accuracy can be obtained as measure of the quality of the inversion.

II. Experimental Data

A. CARABAS-II System

CARABAS-II operates in the lower VHF-band (20–90 MHz) which means that the wavelengths are much longer (3–15 m) than for most other remote-sensing systems. The bandwidth gives a range resolution of about 2.5 m. By using a wide aperture angle, typically an azimuth angle of 70° is used [17], a similar azimuth resolution is achieved.

The antenna system consists of two biconical wideband antennas housed in a dual-boom configuration. A single antenna lobe is formed by true time-delaying on-transmission, whereas the received signal in each antenna is recorded in separate receiver channels. The polarization varies over the aperture but is essentially horizontal within the processed aperture. The antenna has a broad elevation pattern, allowing measurements over most incidence angles, with angles from 45° to 70° typically used for imaging [11].

B. Tönnersjöheden Test Site

The Tönnersjöheden forest research park (latitude: 56°41′ N, longitude: 13°06′ E) is run by the Swedish University of Agricultural Sciences. The park consists mainly of Norway spruce (*Picea abies*) but some Scots pine (*Pinus sylvestris*) and deciduous tree species (e.g., beech *Fagus sylvatica*) are also present. The ground topography is variable with slopes up to about 15° measured on a 50-m grid. The ground elevation varies from 55 to 140 m above sea level.

The ten CARABAS-II images of Tönnersjöheden used in this paper were acquired on May 29, 2002. The separation between adjacent flight directions was between 22° and 67°, as shown in Fig. 1. The flight altitudes were about 3400 m, and the incidence angles for the studied forest areas varied between 46° and 66°. The processed frequency band was 20–80 MHz, and the processed Doppler cone angle was 70°.

Fig. 2 shows the Tönnersjöheden test site imaged with CARABAS-II. This image is created from the average backscatter values of all ten geocoded images with different viewing directions. For comparison, a single image of the same area is shown in Fig. 3. Strong scattering objects like metal wire fences (used to protect young trees from large herbivores such as deer and moose) that are only partially visible in single images are, after averaging of multiple images, easier to detect, and the fences form closed loops in the averaged backscatter image. The improved signal-to-noise ratio also makes it easier to detect weak structures like roads and small open areas. In

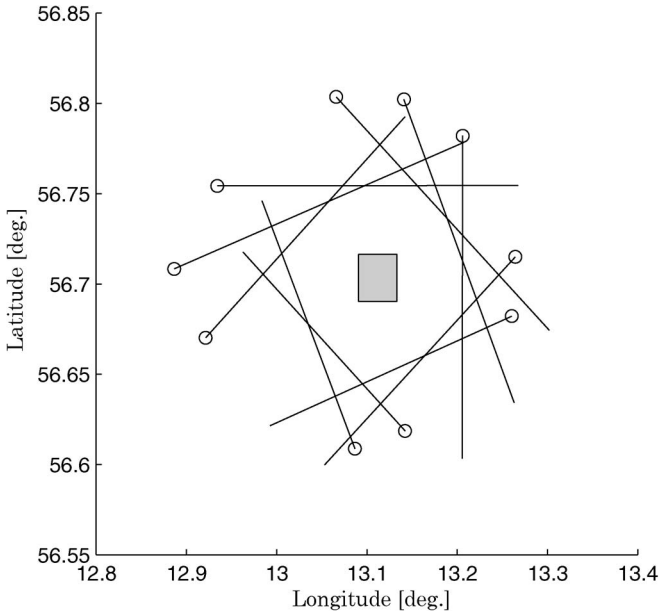

Fig. 1. Flight paths used for acquisition of the ten CARABAS images. Image acquisition started at the points marked with circles. The Tönnersjöheden test site is in the center, and the gray square shows the extent of the image in Fig. 2.

Fig. 2. Mean-value image of the ten CARABAS-II images from the Tönnersjöheden test site. Strong scattering is visible from an overhead powerline going in a straight line from the lower right corner. Image area is 2.5 km by 3 km.

addition, the contrast between lakes, which are the darkest areas, and forested areas with small trees are higher. Most of the area covered by these images consists of forests of varying age, with brighter areas corresponding to higher stem volume.

C. Calibration and Backscatter Measurements

The radiometric calibration of the CARABAS-II images was done using a trihedral reflector with a shortest side with a length of 5 m. The reflector was placed in an open field on horizontal ground and was rotated before each flight pass to align the vertical symmetry plane orthogonal to the flight track. The calibration is estimated to give an absolute accuracy of ± 1 dB [17].

Fig. 3. Single CARABAS-II with flight direction at 182°, i.e., from top to bottom and imaging from the right side of the image, showing the same area as Fig. 2.

The normalized backscattering amplitude s^o [in meters per square meter] was calculated from geocoded CARABAS-II images as [5]

$$s^o = \frac{1}{n}\sum_{k=1}^{n} |DN_k| \frac{\cos \Psi_k}{dadr} \tag{1}$$

where DN_k is the complex number of pixel k, n is the number of pixels within the area for which the backscattering is calculated, Ψ_k is the angle between the normal to the SAR image plane and the normal to the surface plane for pixel k [18], and da and dr are the pixel sizes in azimuth and range. The reasons for using s^o instead of the more commonly used backscattering coefficient σ^o [in square meters per square meter] are presented in Section IV-C.

D. DEMs

In September 2002, measurements of the ground topography were made with the helicopterborne TopEye nadir-looking LIDAR system [19]. The combination of the laser range finder with the helicopter's inertial navigation system and kinematical GPS data gives an accuracy of the 3-D position of the laser echoes of about 10–30 cm. From the LIDAR measurements, a DEM with spatial resolution of 0.25 m was constructed.

As an alternative to the detailed but expensive LIDAR DEM, we also use the Terrain Elevation Databank [20] produced by

the National Land Survey of Sweden. This data set covers the whole country and has a horizontal pixel size of 50 m by 50 m. The DEM is intended to achieve a vertical accuracy with a maximum standard error of less than 2.5 m, but the accuracy can be severely reduced in areas with dense forests.

E. In situ Data

In 1998 and 1999, extensive objectively measured ground data were collected for about 70 stands using The Forest Management Planning Package [21] developed at the Swedish University of Agricultural Sciences (SLU). Within each stand, about ten plots with 10-m radius were placed on a randomly positioned systematic grid. Some of the parameters recorded were number of trees (stem diameter > 5 cm), tree species, and diameter at breast height. An electronic caliper was used to measure diameter and record species code. For a few randomly selected trees, the tree heights were also measured using an inclinometer. The measured stem volume varies from 80 to 700 $\mathrm{m^3ha^{-1}}$, and the average accuracy of the stem-volume estimates have a standard error of about 10%. Out of the 70 stands that were inventoried, 37 are within the area covered by the CARABAS-II images and the high-resolution LIDAR DEM, and these 37 stands are the field data that are used in this paper.

III. Segmentation of SAR Images

Image segmentation is an image-processing technique in which images are divided into statistically homogeneous regions. The number of regions and their size and shape depend on the image data and the algorithm chosen. Our goal with the segmentation is to find forested areas where the stem volume and ground slope are constant. This corresponds to regions where the backscatter is homogenous in each image but the average backscatter amplitude may vary from image to image due to different look directions. Since the goal is to find one region map from all available images, the segmentation algorithm needs to be able to use information from several images simultaneously.

The segmentation algorithm we use is based on simulated annealing optimization [22]–[24]. The idea of simulated annealing is to start from a configuration and perturbate it by a small random change. Every configuration is assigned a cost, and depending on the corresponding change in cost, the new configuration is either accepted or rejected. If the randomly perturbed configuration has lower cost than the current configuration, the new configuration is always accepted. Otherwise, it is accepted with a probability that is dependent on the change in cost and for how long the annealing has been performed. This probability of moving to a combination with higher cost is necessary to avoid the solution being a local minimum close to the initial configuration. The process of testing random perturbations is repeated iteratively until the cost is at minimum. The cooling schedule, i.e., the reduction in probability of accepting a configuration with higher cost, will highly affect the result and the execution time. We have chosen to use slow cooling for a better optimization, which results in high-quality segmentation but long execution times.

The cost function we use for the segmentation is defined as [24], [25]

$$C = C_A + s \cdot C_S \tag{2}$$

where the total cost C is made up by two terms. The term C_A

$$C_A = a_0 + \sum_{k=1}^{M} L_k \sum_{j=1}^{N} N_j \ln \overline{I_{j,k}} \tag{3}$$

is the log likelihood of fit of the segments to the image data assuming fully developed speckle. The log of the mean intensity $\overline{I_{j,k}}$ for region j in image k is multiplied by the number of pixels N_j in the region. The sum for all the N regions is multiplied by the number of looks L_k in image k and is summed for all M images. The parameter a_0 is a constant. The second term in (2) is

$$C_S = \frac{1}{2} \sum_{i} \sum_{j \in \mathrm{Nbhd}(i)} (1 - \delta_{r_i r_j}) \tag{4}$$

where r_i and r_j are the region labels for pixel i and j, $\mathrm{Nbhd}(i)$ is the neighborhood of pixel i, i.e., the eight pixels surrounding pixel i, and $\delta_{r_i r_j}$ is the Kronecker delta (one if $r_i = r_j$ and zero otherwise). Hence, this part increases the cost if a pixel is at the edge of a region. The constant s is used to balance the relative weight of the two terms. Small values of s give many regions with wrinkled edges. A larger value of s means the number of regions is reduced and the regions' borders become straighter. We use a value of s so that the size of the segments are large enough to accurately measure the average backscatter within the segments. The exact value of s to obtain a certain average segment size will vary slightly depending on the images. If a segmentation has too few or too many segments, s is changed until a segmentation with the desired number of segments is obtained.

Before image segmentation, we multilook the CARABAS-II images, which are delivered with 1 m by 1 m pixels, to a pixel size of 5 m by 5 m. By multilooking, the distribution of pixel intensities becomes more like the gamma distribution of multilook speckle upon which the segmentation method is based. The pixel distribution in forested areas in CARABAS-II images has a heavier tail than the exponential distribution that is usually used to describe speckle statistics in single-look SAR images [24], [26]. After multilooking, the equivalent number of looks in the images is about three to four. A side effect of the multilooking is that the computational burden is reduced, but we still have execution times of a few hours on a standard PC for the images covering the Tönnersjöheden test site. The output from the segmentation algorithm is a region map and the averaged backscatter for each region and image. This information is used as measurement data in the optimal estimation method described as follows. The quality of the segmentations is discussed as follows in Section V-A.

IV. Optimal Estimation Method

To retrieve the stem volume from the measured backscatter in the CARABAS-II images, we need a model that relates the backscatter to properties of the forest and imaging system and geometry. This relationship can be expressed as

$$y = F(x, b) + \epsilon \tag{5}$$

where the vector y is the measurements with error ϵ and $F(x, b)$ is the forward model with state vector x and other parameters b. We handle one segment at a time and, hence, use the information in the radar images within a segment to make the retrieval for that segment. The length of the measurement vector y is equal to the number of images, and the values of the elements are the average backscatter values within the segment.

The values of the forward model depend on the quantities to be retrieved which is represented in the state vector x and other parameters given in the vector b. Our state vector x consists of four parameters. Two of these, the stem volume v and the tree height h, are related to forest properties. The two other, the ground slope angle θ_g and aspect angle ϕ_g, are related to the ground topography and describes how much and in what direction the ground slopes. The forward model also utilizes information about the flight headings, incidence angles to the center point of the current segment and a parameter that tells toward which side of the airplane the radar is imaging. These parameters are derived from recorded flight data and are included into the model as the parameter vector b. The reason the ground slope and aspect angle are included in the state vector is that they are not known exactly and depend on the quality of the DEM that is used. By including them in the state vector, we can use the same framework for different DEMs and adjust the *a priori* statistics of these parameters accordingly. It is important that the ground slope angles are not set to fixed values, since they have a large influence on the forward model. When present in the state vector, they can be adjusted according to their *a priori* statistics when the estimation of them is not absolutely correct.

From the CARABAS-II backscatter measurement (including a description of their error statistics), the forward model relating the measurements to the forest properties and the imaging geometry, and *a priori* data for the state vector, we can use the Bayesian approach to find a solution to the inverse problem including an error estimate. The Bayesian approach means that we update our prior knowledge of the forest properties with information from the measurements. We choose to solve for the maximum *a posteriori* solution so that our solution is the state with maximum probability. Assuming Gaussian distributions, we can find the maximum probability state $\hat{x}$ from [16]

$$-\left[\nabla_x F(\hat{x}, b)\right]^{\mathrm{T}} S_\epsilon^{-1}\left[y - F(\hat{x}, b)\right] + S_a^{-1}[\hat{x} - x_a] = 0 \tag{6}$$

where x_a is the *a priori* state vector with covariance matrix S_a and S_ϵ is the covariance matrix for the measurement error ϵ. Matrix transpose is indicated by $^{\mathrm{T}}$ and the inverse of a matrix by $^{-1}$.

A. A priori Data

The *a priori* data for the forest parameters were obtained from the Swedish national forest inventory database. For the region where Tönnersjöheden is located, the average stem volume per hectare for forested areas is 193 $\mathrm{m^3ha^{-1}}$ which we used as expected value in the *a priori* distribution for all segments. The standard deviation for the stem volume was set to 300 $\mathrm{m^3ha^{-1}}$. For the tree height, an expected value of 18 m and a standard deviation of 15 m were used. We choose to use distributions with very high standard deviations for the *a priori* data. This means that the measurements will have large influence on the solution and that the *a priori* data mainly provide a framework to include auxiliary data from other sources, e.g., other sensors or old inventory data, when such data are available.

The two angles θ_g and ϕ_g are estimated from the DEM by least square matching of a sloping plane to the height measurements within the current segment. The true standard deviations for these parameters will vary depending on both topography and quality of the DEM and the image segmentation and were set to have a standard deviation of 2° and 10°, respectively. These values were chosen to be large enough not to underestimate the real values but also small enough so that the information from the DEM is used in the inversion.

B. Measurement Error Statistics

On the basis of empirical measurements [14], the measurements of backscatter amplitude s^o were set to have a normal distributed error with a variance of 0.001. The errors in backscatter are believed to be mainly caused by backlobe leakage and are independent of backscatter amplitude. Measurement errors are treated as being independent, i.e., all covariances between measurements from different images are set to zero, since the effect of the backlobe leakage changes rapidly with flight paths, and the flight directions are separated by at least 22°.

C. Forward Model

A scattering model for coniferous trees on sloping ground was presented in [15]. The model assumes the dominating scattering mechanism is the dihedral ground–stem bounce where the ground is a sloping smooth dielectric plane and the dielectric stem is a vertical cylinder. Both the ground and the stem are assumed to be dielectrically homogeneous. Moreover, the interaction between stems is neglected, and the attenuation due to the canopy is assumed to be constant.

In [14], the model was evaluated, and the error statistics were investigated. It was found that relating the stem volume to the normalized backscattering amplitude s^o instead of the backscattering coefficient σ^o has a few advantages. The normalized backscattering amplitude was shown to be linearly related to the stem volume, and the standard deviation in backscatter between multiple CARABAS-II images was independent of backscatter amplitude and stem volume. The observed variations in backscatter are believed to be mainly caused by backlobe leakage, and it was found reasonable to approximate the noise in s^o as additive Gaussian noise. Theoretically, the backscatter amplitude s^o is proportional to the stem volume in areas where

the stems are resolved, i.e., in sparse forests [5], whereas σ^o is also sensitive to the number density of the trees. However, observations suggest that the backscattering amplitude s^o and the stem volume are highly correlated even in areas where the trees are not fully resolved. We prefer the use of s^o due to the explicit relation to the stem volume and the fact that the noise characteristics are independent of s^o [14].

The forward model $F(x, b)$ relating the normalized backscattering amplitude s^o to forest, system, and imaging variables that we use for inversion can be expressed as

$$s^o = C' v \sqrt{\left\langle k^4 \mathrm{sinc}^2 \left(k \frac{\alpha h}{2} (\cos\theta_{\mathrm{sg}} - \cos\theta_i) \right) \cdot \cos^2(\phi_{\mathrm{sg}} - \phi_i) \right\rangle} + s_{\mathrm{noise}} \quad (7)$$

where the forest variables are the stem volume v, the tree height h, and α which compensates for the fact that the shape of the trunk is not a cylinder but tapers toward the top. A fixed value of $\alpha = 2/3$ was used [15]. The angles θ_{sg}, θ_i, ϕ_{sg}, and ϕ_i are related to viewing geometry and ground slope. The angles with indexes i describe the direction of the incident wave, and the angles with indexes sg describe the direction of the wave going from the stem toward the ground (the geometry is shown in Fig. 1 of [15]).

The other variables in the model are the wavenumber k, a factor C' related to the dielectric properties of the trunk and the ground plane, as well as the incidence angle and an elevated noise level s_{noise} mainly caused by backlobe leakage [14]. Since CARABAS-II has both wide bandwidth and wide antenna beam, the model has to average over these, and this is indicated by the brackets $\langle\rangle$. The forward model (7) is valid for ground slopes up to about 10° and uses the Rayleigh–Gans approximation that the trunks can be modeled as long thin cylinders [15].

Both of the variables C' and s_{noise} need to be calibrated for. Variations in moisture content in both soil and stems, for instance, caused by weather and topography, will affect C' and, hence, the backscattering strength for a certain stem volume. The noise level s_{noise} depends on the surrounding areas and the effects of external radio-frequency interference and will vary with both geographic location and on the flight path. In this paper, both these variables are treated as constants and are estimated by ordinary least square fitting to the *in situ* data. The remaining noise after subtraction of the constant noise level s_{noise} is modeled into the measurement error ϵ.

D. Levenberg–Marquardt Method

To find the maximum *a posteriori* solution for (6), which for our forward model is a nonlinear least squares problem, we use the Levenberg–Marquardt method [27]. The solution of (6) is iteratively found from [16]

$$x_{i+1} = x_i + \left[(1+\gamma) S_a^{-1} + K_i^{\mathrm{T}} S_\epsilon^{-1} K_i\right]^{-1} \times \left\{ K_i^{\mathrm{T}} S_\epsilon^{-1} \left[y - F(x_i, b) \right] - S_a^{-1} [x_i - x_a] \right\} \quad (8)$$

where the next solution x_{i+1} is derived from the current solution x_i, the measurement vector y, its error covariance matrix S_ϵ, the *a priori* vector x_a, its covariance matrix S_a, and the predicted backscatter from the current state vector and the forward model $F(x_i, b)$. The Jacobian $K_i = K(x_i) = \nabla_x F(x_i, b)$ is numerically calculated by disturbing the forward model around the vector x_i.

We start the iteration from $x_0 = x_a$ [16]. The parameter γ which is updated in each iteration controls the continuous transition from steepest descent to inverse Hessian as the minimum is approached [27]. We stop the iteration of (8) when the difference between the previous and the new state vector is an order of magnitude smaller than the estimated error. We also check that the found solution is not a spurious solution from local minima by calculating a chi-square test comparing the retrieval with the measurement. Segments where the difference is statistically significant, and also segments for which the iteration fails to converge within reasonable time, are discarded. This rarely happens for segments in forested areas and is most often caused by man-made objects for which the forward model is not applicable.

E. Error Estimation

The *a posteriori* covariance matrix $\widehat{S}$ after the inversion is calculated from [16]

$$\widehat{S} = \left[S_a^{-1} + K_i^{\mathrm{T}} S_\epsilon^{-1} K_i \right]^{-1}. \quad (9)$$

The diagonal elements of $\widehat{S}$ are the *a posteriori* variances of the variables in the state vector. Of these, we are mostly interested in the upper left element $\widehat{S}_{11}$, i.e., the *a posteriori* variance of the stem volume v.

The measurement response, i.e., the diagonal elements of [16]

$$A = \widehat{S} K_i^{\mathrm{T}} S_\epsilon^{-1} K_i \quad (10)$$

indicates the amount of information about the state vector that originates from the measurements. A value close to unity indicates that most of the information comes from the measurements, while a value close to zero means that the *a priori* data are dominating the retrieved state vector.

The measurement response for the stem volume v is almost always very close to unity, with average value above 0.99 and the lowest values at about 0.7. This indicates that the measurements dominate the solution, which is what we prefer considering the very wide *a priori* distribution for this variable. The measurement response for the tree height h shows more variability and is approximately uniformly distributed from zero to unity. This is not unexpected, since the tree-height-measurement accuracy using CARABAS-II is low, and the tree height does not affect the model-predicted backscatter when the ground is flat and horizontal. Finally, the measurement response for the two ground slope angles θ_g and ϕ_g are below 0.5 for all segments.

V. Results

We evaluate the results from our segmentation and inversion method by comparing with simpler methods that have

been used previously. These include average backscatter from multiple images, maximum backscatter from multiple images, and single-image retrieval. Retrieval of stem volume from the ten single images gives a correlation between backscatter amplitude and *in situ* measured stem volume that varies from $R^2 = 0.45$ to $R^2 = 0.77$. The root-mean-square errors (rmses) are 55–131 $\mathrm{m^3ha^{-1}}$, and the maximum retrieval errors are 168–461 $\mathrm{m^3ha^{-1}}$. This large variation can be explained by differences in image noise and that the topography in Tönnersjöheden makes some flight paths more favorable than others [15]. Clearly, a single image would not be guaranteed to meet the requirements of most users, and even with knowledge about the ground topography, it is very difficult to determine which flight path will generate the image which gives the best result.

In this section, we first investigate the results obtained using all the available images and the high-resolution DEM. Aside from the model-based inversion presented in this paper, we also show results from using the average and the maximum backscatter values for the segments to allow comparison with the method proposed in [7]. We then reduce the data, i.e., use the less accurate DEM and fewer images, to show how the model-based inversion performs with data quantities that are more realistic for large-scale mapping.

A. Model-Based Retrieval of Stem Volume

Within the area covered by the DEM, there are 37 forest stands with ground-measured stem volume and tree height. The stem volumes for the stands were calculated as the area- and variance-weighted average of the stem volumes of the segments, i.e.,

$$v_{\mathrm{model}} = \frac{\sum_{i=1}^{n} \frac{n_i v_i}{\widehat{S}_{11}^i}}{\sum_{i=1}^{n} \frac{n_i}{\widehat{S}_{11}^i}} - \frac{s_{\mathrm{noise}}}{C'} \tag{11}$$

where n_i is the number of pixels within segment i, v_i is the retrieved stem volume, and $\widehat{S}_{11}^i$ is the *a posteriori* variance for the stem volume for segment i. For segments which cross a stand border, only the parts of the segments that are within the stand are included. Due to the limited *in situ* data with only 37 stands, we use the same data both to estimate s_{noise} and C' (using ordinary least square fitting) and to evaluate the stem-volume retrieval result.

The result after applying our image segmentation and inversion methods is shown in Fig. 4 as a plot of *in situ* measured stem volume versus retrieved stem volume. The correlation coefficient is $R^2 = 0.90$, and the rmse in estimated stem volume is 54 $\mathrm{m^3ha^{-1}}$. The maximum retrieval error is 121 $\mathrm{m^3ha^{-1}}$.

Since we have no method to objectively evaluate the quality of the segmentations, we compare the stem-volume retrieval results from several segmentations with identical input data. The simulated annealing algorithm only finds an approximative solution to the minimization problem, but if the end result is similar, we believe the segmentation method is a good one, even if there are small differences in the segmentations. Several segmentations with identical input data resulted in slightly different segmentations, e.g., the number of segments were between 1799 and 1839. However, the stem-volume retrievals from the different segmentations differed very little. The correlation coefficient varied from $R^2 = 0.88$ to $R^2 = 0.91$, and the rmse in estimated stem volume was between 54 and 64 $\mathrm{m^3ha^{-1}}$. An example of a segmentation is shown in Fig. 5, where the images that made up Fig. 2 have been segmented and the inversion method has been applied.

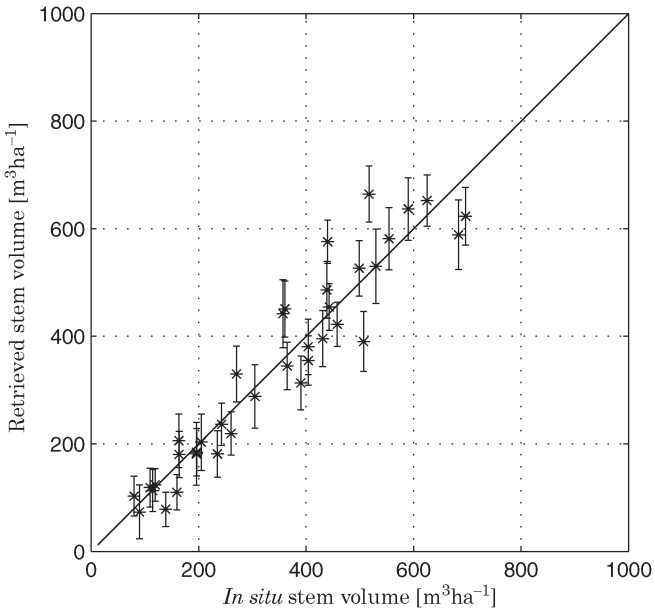

Fig. 4. Model-based retrieval of stem volume using ten images and the high-resolution LIDAR DEM ($R^2 = 0.90$). The error bars indicate the standard deviation of the *a posteriori* stem-volume estimates. The average accuracy of the stem-volume estimates has a standard error of about 10%.

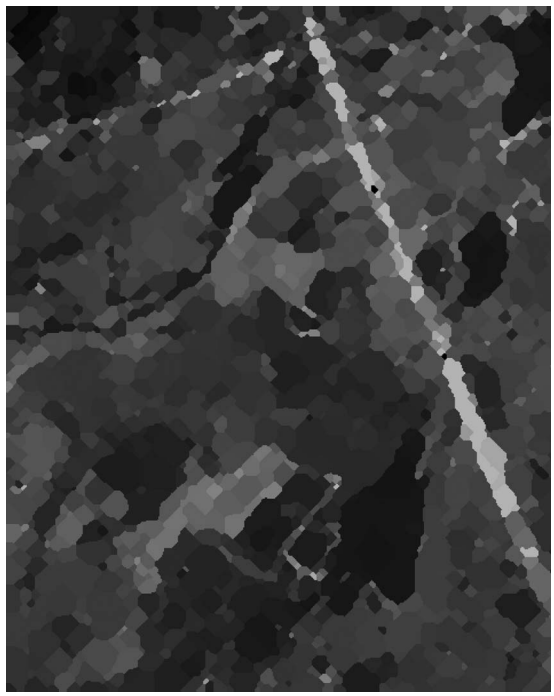

Fig. 5. Stem-volume map after segmentation and model-based inversion of the images in Fig. 2.

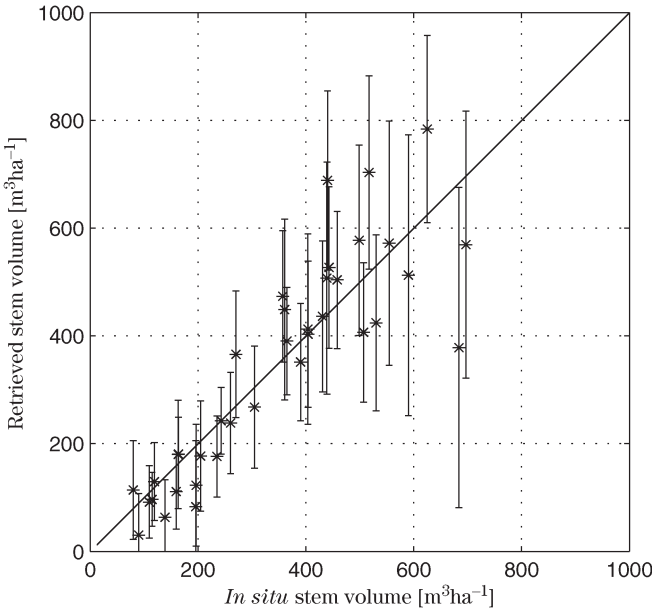

Fig. 6. Stem-volume retrieval using the average backscatter from ten images ($R^2 = 0.76$). The error bars indicate one standard deviation. The average accuracy of the *in situ* stem-volume estimates has a standard error of about 10%.

B. Using Average Backscatter Value

For stands on flat and horizontal ground, the backscatter amplitude is proportional to the stem volume according to (7), and averaging the backscattering from multiple images improves the estimated stem volume [14]. The stem volumes for the stands were calculated as the area-weighted average of the mean amplitude of the segments, i.e.,

$$v_{\text{average}} = \frac{1}{C'} \sum_{i=1}^{n} \frac{n_i}{N} \left\langle s_i^o \right\rangle - \frac{s_{\text{noise}}}{C'} \tag{12}$$

where n_i is the number of pixels within segment i, N is the number of pixels within the stand, and $\langle s_i^o \rangle$ is the average backscatter amplitude from all images within segment i. For segments which cross a stand border, only the parts of the segments that are within the stand are included. We use the same method to estimate s_{noise} and C' as for the model-based inversion.

The result when using the average backscatter amplitude is shown in Fig. 6. The correlation coefficient is $R^2 = 0.76$, and the rmse in estimated stem volume is 85 m^{3}ha^{-1}. The maximum retrieval error is as large as 314 m^{3}ha^{-1}. This method has its largest problem for high stem volumes which are underestimated when the ground is sloping. Due to the lower backscatter within these stands, stands with high stem volumes and less ground slope are overestimated due the way we calculate the regression constant C^{prime}. This causes a larger spread in retrieved stem volume and the large maximum retrieval error. For stands with low stem volume, this method performs almost as well as the optimal estimation model.

C. Using Maximum Backscatter Value

In [7], the maximum backscatter from multiple images were assumed to be close to the backscatter that would be obtained from the same stem volume on horizontal ground. The images were divided into segments using a DEM to find areas with constant ground slope. Here, we use the image segmentation presented earlier which differs in that it finds segments that have homogeneous backscatter, but homogeneous backscatter also means constant ground slope. We calculate the stem volume $v_{\max}$ as

$$v_{\max} = \frac{1}{C'} \sum_{i=1}^{n} \frac{n_i}{N} \left\lceil s_i^o \right\rceil - \frac{s_{\text{noise}}}{C'} \tag{13}$$

where n_i is the number of pixels within segment i, N is the number of pixels within the stand, and $\lceil s_i^o \rceil$ is the segment backscatter from the image with the highest backscatter. Once again, we use the *in situ* data to estimate the noise level s_{noise} and the factor C' using ordinary least square fitting in the same way as for the two previous methods.

Taking the maximum segment backscatter from the images and averaging within the stands provides better results than the average backscatter value method, but it is less accurate than the optimal estimation method. The correlation coefficient is $R^2 = 0.83$, the rmse in estimated stem volume is 72 m^{3}ha^{-1}, and the maximum retrieval error 208 m^{3}ha^{-1}. This is shown in Fig. 7.

This method is less robust, and image artifacts can affect the result. In this case, the stand with the lowest stem volume is highly overestimated because the measured backscatter is dominated by an artifact. Since this method is sensitive to the extreme values of scattering, more images increase the risk of an image artifact in any of the images, so these problems become worse the more images are used. Moreover, the spread of the measurements increases with increasing stem volumes which indicates that the ground slope effect is less compensated than when using the optimal estimation method. Finally, there is no obvious way to make an error assessment of the retrieved stem volume.

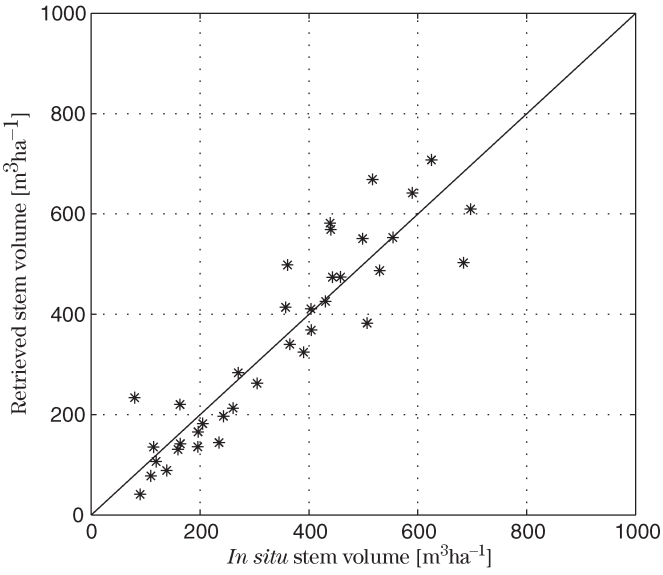

Fig. 7. Stem-volume retrieval using the maximum backscatter from ten images ($R^2 = 0.83$). The average accuracy of the *in situ* stem-volume estimates has a standard error of about 10%.

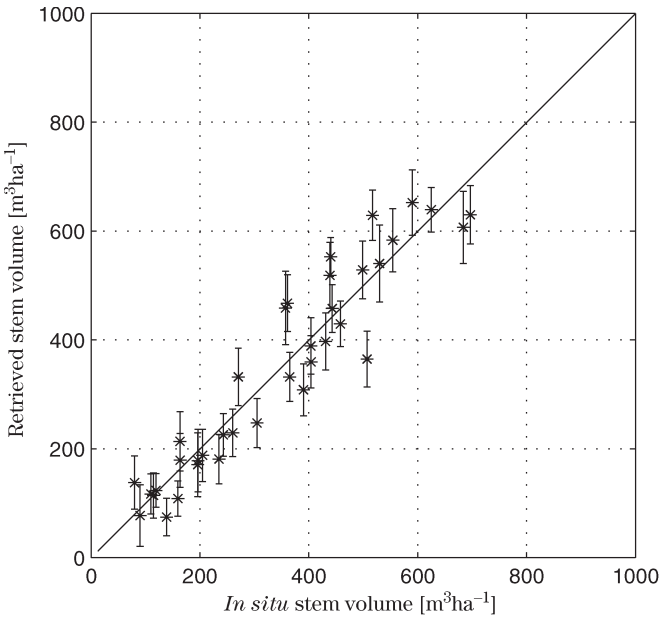

Fig. 8. Model-based retrieval of stem volume using ten images and DEM from the National Land Survey of Sweden ($R^2 = 0.90$). The error bars indicate the standard deviation of the *a posteriori* stem-volume estimates. The average accuracy of the *in situ* stem-volume estimates has a standard error of about 10%.

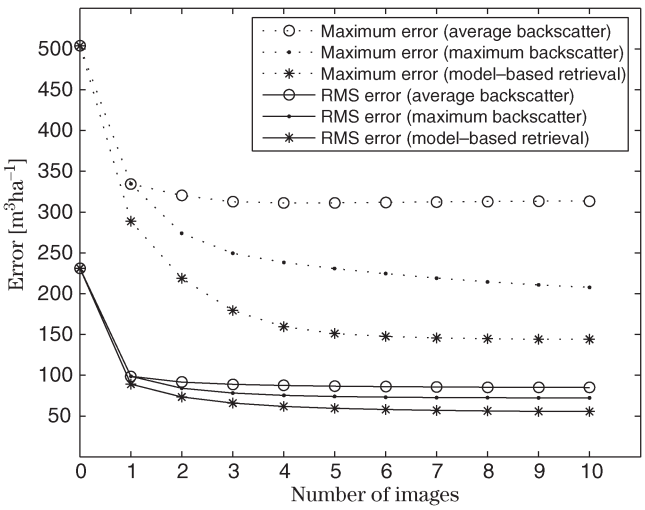

Fig. 9. Average retrieval errors for the three methods when using different number of images. The case with zero images indicates retrieval errors when using the *a priori* data as retrieved data.

D. Reduced Data

The data available at Tönnersjöheden, i.e., ten CARABAS-II images and a very detailed DEM, are more extensive than can be expected in a larger mapping project using CARABAS-II. To illustrate the performance of the presented method using segmentation and model-based inversion, we show the result with less data, e.g., a coarser and less accurate DEM and fewer images.

1) Less Accurate DEM: First, we replace the LIDAR DEM with the national 50-m-grid DEM which we bilinearly interpolate to match the pixel size of the segmentation and, thus, simplify calculation of slopes within each segment. Using all of the ten images and the same segmentation as earlier, we get almost as good results as shown in Fig. 8. In this case, the correlation coefficient is $R^2 = 0.90$, and the rmse in estimated stem volume is 55 m^{3}ha^{-1}. These values are almost identical to when using the LIDAR DEM, while the maximum retrieval error of 144 m^{3}ha^{-1} is slightly higher.

2) Fewer Images: We now study the performance when using different number of images. For easier comparison of the different methods, we use the same segmentation of the ten images as was used earlier also for the combinations with fewer images. Fig. 9 shows the maximum and the rms retrieval errors for different number of images. The *a priori* data and the 50-m-grid DEM are the same as in the previous section, so with ten images, we have the same case as was shown in Fig. 8. The case with zero image is when using the expected value of the stem volume in the *a priori* data (193 m^{3}ha^{-1}) as retrieved stem volume for all stands. For the situations with one to nine images, the retrieval accuracies for all combinations of images have been computed, and Fig. 9 shows the average retrieval errors. For comparison, the corresponding errors when using the average or the maximum backscatter are also shown in Fig. 9.

One of the images (flight direction 92°) appears to have favorable viewing geometry with respect to the ground topography and is the single image that gives the lowest retrieval errors. This image is overrepresented in image combinations with low errors. Apart from that, there is no clear indication that any particular combinations of images are better than the other, and all images are represented in combinations of images that give rmses below 50 m^{3}ha^{-1} when using the model-based retrieval method. The model-based retrieval method seems less sensitive to the choice of flight directions, and the errors vary less for different combinations of images. In particular, when using the average backscatter, the errors depend a lot on which image combination was used.

When using only one image, the model-based retrieval gives lower errors than without any slope compensation. The rmses are 55–117 m^{3}ha^{-1} as compared to 55–131 m^{3}ha^{-1} when directly relating the average backscatter amplitude within a stand to the stem volume. The maximum retrieval errors 171–369 m^{3}ha^{-1} are also, on average, lower than without slope compensation. With more images, the average errors become lower with all three methods. However, the model-based method gives more rapid reduction in errors and always performs better than the other two methods. Model-based inversion with three images gives, on average, a lower rmse than using the maximum backscatter from all ten images, while one image is enough to give a lower average rmse than the method using the average backscatter from all ten images. The same result is observed for the maximum error. These average errors demonstrate that the model-based inversion gives higher retrieval accuracy, on average, than the other methods, although the retrieval error using few images still varies depending on exactly which of the images are chosen.

When using four images, the rmse varies from 43 to 82 m^{3}ha^{-1}. Hence, even for the worst combination of four images, the rmse is lower than when using the average backscatter from ten images. Fig. 10 shows an example of model-based

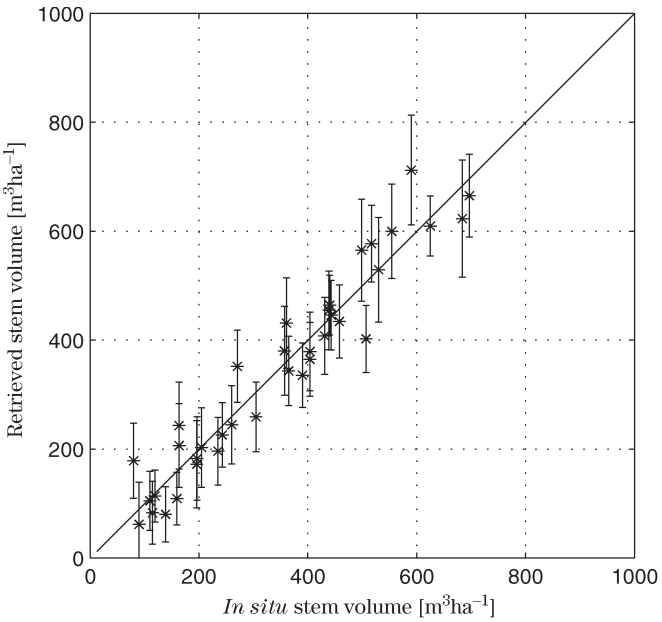

Fig. 10. Example of segmentation and model-based stem-volume retrieval using only four of the images and the DEM from the National Land Survey of Sweden ($R^2 = 0.93$). The error bars indicate estimates of one standard deviation. The average accuracy of the *in situ* stem-volume estimates has a standard error of about 10%.

retrieval result when using four adjacent flight directions (47°, 71°, 92°, and 137°). For this example, which is based on a segmentation of only the four images, the correlation coefficient is $R^2 = 0.93$, and the rmse in estimated stem volume is 48 m^{3}ha^{-1}. The maximum retrieval error is 111 m^{3}ha^{-1}. The similarity with Fig. 4 indicates that four images often can be enough.

VI. Discussion and Conclusion

In this paper, we have presented the first systematic approach to combine information from multiple CARABAS-II images with available ground-topography data with an aim to produce a stem-volume map. Using image segmentation and optimal estimation method, we are able to remove most of the ground-topography influence on the CARABAS-II backscatter and achieve similar accuracy as obtained previously for flat and horizontal ground. A coarse DEM with 50-m resolution seems to be accurate enough to provide the ground-topography information that is needed. The number of images needed for operational stem-volume mapping is an open question which requires much more image data and knowledge about user-requirements to answer. However, for the data set used in this paper, four images yield almost as accurate retrieval accuracy as ten images and requiring four images is not a prohibiting factor for large-scale mapping with CARABAS-II as demonstrated in [28]. Stem-volume retrieval using the model-based inversion is also superior to the simpler image combination methods using either average or maximum backscatter that have earlier been proposed.

Two effects of ground topography still require further study. First, for slopes steeper than about 10°, according to the scattering model, the dihedral bounce is not as dominating, and the ground–trunk–ground triple bounce becomes important [15]. This would have to be modeled and studied in mountain areas. However, for large areas of the boreal region, the coniferous forests are located on rather flat ground, and this is not a pressing issue.

The other issue is small-scale topography where the ground topography is not well represented by one sloping ground plane. For instance, for trees standing on a ridge, the ground would be better described by different planes depending on the imaging direction. Since the ground bounce can take place up to a distance of about the double tree height away from the tree position, variations in the ground topography within this distance from the tree will affect the scattering. In addition, nonvertical stems are a similar problem where the scattering geometry is not well described by the same sloping ground plane for all imaging directions.

Other improvements would be to include variations in soil moisture and dielectric constant of the trunks in the forward model. Meteorological data and the DEM could be used to provide estimates of these. Future forward models also need to account for tree species with larger branches and, thus, other backscattering properties. The optimal estimation method can then be used as a framework for including other types of data.

Execution time for segmentation and inversion is about 15 h for 3 km by 2.5 km area on a standard PC with all code implemented in MATLAB. Tuning of algorithm parameters combined with faster code implementation can probably reduce execution time to be less than an hour in a finished product.

Using the proposed method to mitigate influence from ground topography on the CARABAS-II backscatter, backlobe leakage is the limiting factor when using CARABAS-II for stem-volume retrieval of coniferous forests. This issue needs to be addressed with technical improvement of future versions of the system. A method to calibrate for variations in noise level is also needed.

Acknowledgment

The authors would like to thank P. Eriksson of Chalmers University of Technology, the CARABAS group at FOI, Linköping, and J. Fransson and M. Magnusson of the Department of Forest Resource Management, SLU, Umeå.

References

[1] H. Israelsson, L. M. H. Ulander, J. L. H. Askne, J. E. S. Fransson, P.-O. Frölind, A. Gustavsson, and H. Hellsten, "Retrieval of forest stem volume using VHF SAR," *IEEE Trans. Geosci. Remote Sens.*, vol. 35, no. 1, pp. 36–40, Jan. 1997.

[2] F. Walter, "Extraction of forest tree volume from CARABAS SAR data," *Scand. J. For. Res.*, vol. 12, no. 4, pp. 370–374, 1997.

[3] M. L. Imhoff, S. Carson, and P. Johnson, "A low-frequency radar experiment for measuring vegetation biomass," *IEEE Trans. Geosci. Remote Sens.*, vol. 36, no. 6, pp. 1988–1991, Nov. 1998.

[4] J. E. S. Fransson, F. Walter, and L. M. H. Ulander, "Estimation of forest parameters using CARABAS-II VHF SAR data," *IEEE Trans. Geosci. Remote Sens.*, vol. 38, no. 2, pp. 720–727, Mar. 2000.

[5] G. Smith and L. M. H. Ulander, "A model relating VHF-band backscatter to stem volume of coniferous boreal forest," *IEEE Trans. Geosci. Remote Sens.*, vol. 38, no. 2, pp. 728–740, Mar. 2000.

[6] P. Melon, J. M. Martinez, T. Le Toan, L. M. H. Ulander, and A. Beaudoin, "On the retrieving of forest stem volume from VHF SAR data: Observation and modeling," *IEEE Trans. Geosci. Remote Sens.*, vol. 39, no. 11, pp. 2364–2372, Nov. 2001.

[7] J. E. S. Fransson, G. Smith, F. Walter, A. Gustavsson, and L. M. H. Ulander, "Estimation of forest stem volume in sloping terrain using CARABAS-II VHF SAR data," *Can. J. Remote Sens.*, vol. 30, no. 4, pp. 651–660, Aug. 2004.
[8] B. Hallberg, G. Smith-Jonforsen, and L. M. H. Ulander, "Measurements on individual trees using multiple VHF SAR images," *IEEE Trans. Geosci. Remote Sens.*, vol. 43, no. 10, pp. 2261–2269, Oct. 2005.
[9] A. A. Kononov and M.-H. Ka, "Model-associated forest parameter retrieval using VHF SAR data at the individual tree level," *IEEE Trans. Geosci. Remote Sens.*, vol. 46, no. 1, pp. 69–84, Jan. 2008.
[10] T. Häme, A. Salli, and K. Lahti, "Estimation of carbon storage in boreal forests using remote sensing data," in *Proc. Finnish Res. Programme Clim. Change*, M. Kanninen and P. Anttila, Eds., Mar. 1992, pp. 250–255.
[11] H. Hellsten, L. M. H. Ulander, A. Gustavsson, and B. Larsson, "Development of VHF CARABAS II SAR," in *Proc. SPIE Radar Sensor Technol.*, Orlando, FL, Apr. 8–9, 1996, vol. 2747, pp. 48–60.
[12] M. Magnusson and J. E. S. Fransson, "Combining airborne CARABAS-II VHF SAR data and optical SPOT-4 satellite data for estimation of forest stem volume," *Can. J. Remote Sens.*, vol. 30, no. 4, pp. 661–670, 2004.
[13] H. I. Israelsson, L. M. H. Ulander, T. Martin, and J. I. H. Askne, "A coherent scattering model to determine forest backscattering in the VHF-band," *IEEE Trans. Geosci. Remote Sens.*, vol. 38, no. 1, pp. 238–248, Jan. 2000.
[14] K. Folkesson, G. Smith-Jonforsen, and L. M. H. Ulander, "Validating backscatter models for CARABAS SAR images of coniferous forests," *Can. J. Remote Sens.*, vol. 34, no. 5, pp. 480–495, 2008.
[15] G. Smith-Jonforsen, L. M. H. Ulander, and X. Luo, "Low VHF-band backscatter from coniferous forests on sloping terrain," *IEEE Trans. Geosci. Remote Sens.*, vol. 43, no. 10, pp. 2246–2260, Oct. 2005.
[16] C. D. Rodgers, "Inverse methods for atmospheric sounding," in *Optimal Methods for Non-Linear Inverse Problems*. Singapore: World Scientific, 2000.
[17] L. M. H. Ulander, P.-O. Frölind, and T. Martin, "Processing and calibration of ultra-wideband SAR data from CARABAS-II," in *Proc. CEOS SAR Workshop*, Toulouse, France, Oct. 26–29, 1999, pp. 273–278.
[18] L. M. H. Ulander, "Radiometric slope correction of synthetic-aperture radar images," *IEEE Trans. Geosci. Remote Sens.*, vol. 34, no. 5, pp. 1115–1122, Sep. 1996.
[19] H. Sterner, "Helicopter aerial laser ranging," in *Proc. 3rd EARSeL Workshop LIDAR Remote Sens. Land Sea*, Tallin, Estonia, Jul. 17–19, 1997, pp. 113–118.
[20] Lantmäteriet, GSD-Terrain elevation databank, 2006. [Online]. Available: http://www.lantmateriet.se/
[21] B. Jonsson, J. Jacobsson, and H. Kallur, "The forest management planning package. Theory and application," Faculty Forestry, Swedish Univ. Agric. Sci., Umeå, Sweden, Tech. Rep. S-901 83, 1993. Studia Forestalia Suecica No. 189.
[22] N. Metropolis, A. Rosenbluth, M. Rosenbluth, A. Teller, and E. Teller, "Equation of state calculations by fast computing machines," *J. Chem. Phys.*, vol. 21, no. 6, pp. 1087–1092, Jun. 1953.
[23] S. Kirkpatrick, C. D. Gellat, Jr., and M. Vecchi, "Optimization by simulated annealing," *Science*, vol. 220, no. 4598, pp. 671–680, May 1983.
[24] C. Oliver and S. Quegan, "Understanding synthetic aperture radar images," in *RCS Classification and Segmentation*. Norwood, MA: Artech House, 1998.
[25] K. Folkesson, "Segmentation of radar images for remote sensing of forests," Dept. Radio Space Sci., Chalmers Univ. Technol., Göteborg, Sweden, Tech. Rep. S-412 96, 2005.
[26] J. A. Jackson and R. L. Moses, "Clutter model for VHF SAR imagery," in *Proc. SPIE Algorithms Synth. Aperture Radar Imagery XI*, 2004, vol. 5427, pp. 271–282.
[27] W. H. Press, S. A. Teukolsky, W. T. Vetterling, and B. P. Flannery, "Numerical recipes," in *Modeling of Data*. Cambridge, U.K.: Cambridge Univ. Press, 1992.
[28] L. M. H. Ulander, A. Gustavsson, J. E. S. Fransson, M. Magnusson, G. Smith-Jonforsen, K. Folkesson, B. Hallberg, and L. Eriksson, "Mapping of wind-thrown forests using the VHF-band CARABAS-II SAR," in *Proc. IEEE IGARSS*, Denver, CO, Jul. 31–Aug. 4 2006, pp. 3684–3687.

Klas Folkesson received the M.Sc. degree in engineering physics and the Lic.Eng. degree from Chalmers University of Technology, Göteborg, Sweden, in 2002 and 2005, respectively, where he is currently working toward the Ph.D. degree.

His main research is in the area of microwave remote sensing of forests, with emphasis on low-frequency SAR.

Gary Smith-Jonforsen received the B.A. degree in natural sciences (physics) from the University of Cambridge, Cambridge, U.K., in 1994, the M.Sc. degree in astronautics and space engineering from Cranfield University, Cranfield, U.K., in 1995, and the Ph.D. degree from Chalmers University of Technology, Göteborg, Sweden, in 2001.

From 2001 to 2006, he was an Assistant Professor with Chalmers University of Technology, where he worked on radar remote sensing of forests using UHF/VHF SAR. He is currently with Saab AB, Saab Microwave Systems, Göteborg, where he works on the development of airborne radar systems.

Lars M. H. Ulander (S'86–M'90–SM'04) received the M.S. degree in engineering physics and the Ph.D. degree in electrical and computer engineering from Chalmers University of Technology (CTH), Göteborg, Sweden, in 1985 and 1991, respectively.

Since 1995, he has been with the Swedish Defence Research Agency (FOI), Linköping, Sweden. He is currently the Director of Research in radar signal processing with the Department of Radar Systems, FOI, as well as an Adjunct Professor in radar remote sensing with the Department of Radio and Space Science, CTH. His research area is in synthetic aperture radar, signal processing, electromagnetic scattering, and remote-sensing applications. He is the author or coauthor of about 170 professional publications, of which more than 35 are in refereed journals. He is the holder of five patents.

Dr. Ulander is a member of the Remote Sensing Committee at the Swedish National Space Board. He is listed in *Who's Who in Electromagnetics*.